行政院國家科學委員會專題研究計畫成果報告

※※※※※※※※※※※※※※※※※※※※※※※※※※※※※※※※※※
※　　　　　　　　　　　　　　　　　　　　　　　　　　　　　　　　※
※鹼金族與氫氣反應之氣體動力學研究（中法合作計畫）※
※　　　　　　　　　　　　　　　　　　　　　　　　　　　　　　　　※
※※※※※※※※※※※※※※※※※※※※※※※※※※※※※※※※※※

計畫類別：個別研究計畫

計畫編號：NSC 88-2113-M-002-011

執行期間：87 年 8 月 1 日至 88 年 7 月 31 日

個別型計畫：計畫主持人：林金全
　　　　　　共同主持人：

整合型計畫：總計畫主持人：
　　　　　　子計畫主持人：

註：整合型計畫組報告與子計畫成果報告請分開編印各成一冊，彙整一起繳送國科會。

處理方式：☑可立即對外提供參考
（請打 V）☐一年後可對外提供參考
　　　　　☐兩年後可對外提供參考
　　　　　（必要時，本會得展延發表時限）

執行單位：國立台灣大學化學系

中華民國 89 年 3 月 24 日

關鍵字：反應動力學；雷射誘發螢光；能量儲存

我們自 87.8.1-88.7.31 執行國科會專題計畫，鹼金族與氫氣反應之氣體動力學研究。在 87 年中已完成的結果有：

1. Y. R. Ou, D. K. Liu, and K.C. Lin "Ab initio calculation for potential energy surfaces relevant to the microscopic reaction pathways for $Mg(3s3p^1P_1)+H2 \rightarrow MgH(^2\Sigma^+)+H$", J. Chem. Phys, 108 (4), 1475(1998).

2.C. F. Nien, and K. C. Lin "Kinetic investigation of the quenching of $Mg(3s3p^1P_1)$atoms in collisions with CH_4 over the temperature range from 660 to 850 K", American Institute of Physics, 109, 18, 7821(1998).

Keyword :

reaction dynamics ; laser-induced fluorescence ; product energy disposal

We have accomplished the first-year task (contract no.NSC88-2113-M-002-011) of a three-year term project. The results lead to several papers published. They are listed as follow :

1. Y. R. Ou, D. K. Liu, and K.C. Lin "Ab initio calculation for potential energy surfaces relevant to the microscopic reaction pathways for $Mg(3s3p^1P_1)+H2 \rightarrow MgH(^2\Sigma^+)+H$", J. Chem. Phys, 108 (4), 1475(1998).

2.C. F. Nien, and K. C. Lin "Kinetic investigation of the quenching of $Mg(3s3p^1P_1)$atoms in collisions with CH_4 over the temperature range from 660 to 850 K", American Institute of Physics, 109, 18, 7821(1998).

Time-resolved investigation of the quenching of $Mg(3s3p\ ^1P_1)$ atom in collisions with CH_4 over the temperature range from 660 to 850 K

Chia-Fu Nien and King-Chuen Lin[a)]
Department of Chemistry, National Taiwan University, Taipei, and Institute of Atomic and Molecular Sciences, Academia Sinica, Taipei, Taiwan 106, Republic of China

(Received 10 March 1998; accepted 4 August 1998)

Temperature dependence of the quenching efficiency of $Mg(3s3p\ ^1P_1)$ by CH_4 collision in the Ar bath gas has been studied over the temperature range of 660–850 K, using a pump–probe technique with time-resolved laser-induced fluorescence (LIF) as detection. The obtained thermal rate coefficients are attributed to physical and chemical quenching. The former contribution is evaluated to be less than 6.7×10^{-11} cm^3 molecule^{-1} s^{-1}, while the latter one is $(0.59-1.12)\times10^{-11}\exp(5.75-6.54\ \text{kcal mol}^{-1}/RT)$ cm^3 molecule^{-1} s^{-1} (R is gas constant; T is temperature). The chemical reaction dominates over the exit channels, especially in the low temperature. The negative temperature dependence indicates the existence of a depth-well intermediate. The observed depth-well energy below the reactants is about twice as small as that evaluated theoretically. This bound state is anticipated to locate in the region of surface crossing between the excited and the ground states. We adopted several models to account for the kinetic data as a function of temperature. The orbiting and absorbing-sphere models cannot be validly applied to the current system. The angle-dependent line of normals (ADLN) model takes into account the angular dependence of the threshold energy. The ADLN fit to the measured kinetic data is consistent with the insertion mechanism reported previously, which shows energetic preference to the end-on attack. © *1998 American Institute of Physics.* [S0021-9606(98)00942-8]

I. INTRODUCTION

The way to cleave alkyl C–H bonds in the hydrocarbons by metal atoms has been an attractive subject in reaction dynamics, not only due to fundamental interest but also for the practical application in catalysis. Methane is the smallest, but stable, hydrocarbon. Methane, like H_2, has been identified as an inefficient quencher toward the excited alkali–metal atoms; its lowest unoccupied molecular orbital is the antibonding σ^* orbital.[1,2] However, it differs in reactivity when the metal–atom excitation energy exceeds the required exothermic threshold. For instance, studies have revealed that the mixture of highly excited K-atom vapor and H_2 may yield the KH product. When the mixture is replaced by CH_4 no significant chemical reaction is observed, although the bond strength of C–H in methane is weaker than that of H–H.[3,4] On the other hand, both H_2 and CH_4 may feasibly react with the Mg $3s3p\ ^1P_1$ atom to yield MgH.[5–14] In this sense, to study the reaction of $Mg(3s3p\ ^1P_1)$ with CH_4 is chemically interesting.

In the early 1980s Breckenridge and co-workers investigated the reactions of $Mg(3\ ^1P_1)$ with a series of alkane and alkene hydrocarbons.[6,7] In the reactions, MgH rotational populations had presented a bimodal distribution, in which the deconvoluted low rotational components were almost identical. Thus, it was suggested that a nearly linear Mg–H–C configuration might be the predominant mechanism, since the bond rupture in this manner was least affected by the local molecular environment. Nevertheless, in subsequent studies, they also noted that other reaction pathways including Mg insertion into the C–H bond of the polyatomic reactant should not be ruled out.[14,15] In a recent study on $Mg(3\ ^1P_1)+CH_4$ reaction dynamics, Kleiber and coworkers affirmed the dominance of the Mg insertion mechanism by using a far-wing scattering technique.[10] The MgH low-N and high-N distributions were measured to originate from the same mechanism controlled by the exit channel branching, but independent of how and where the $MgCH_4$ complex was excited in the entrance channel. In our measurement of temperature dependence, the shapes of bimodal rotational distributions were found to be the same within the experimental error.[13] The conclusion also supported the insertion mechanism. According to *ab initio* potential surface calculation by Chaquin *et al.*,[16] a substantial potential barrier of 35 kcal mol^{-1} may be encountered as $Mg(3\ ^1P_1)$ approaches CH_4 along a collinear Mg–H–C axis. In contrast, the insertion pathway may suffer the lowest energy barrier—$<$6.9 kcal mol^{-1}. Considering the reported geometry of the transition state, Breckenridge further suggested that the most favorable mode of C–H bond side-on attack should be highly asymmetric and H atom centered.[14] $Mg(p\pi)-CH(\sigma^*)$ overlap occurs closer to the H atom to avoid repulsion from the other C–H bonds. In view of these studies, the $Mg(3\ ^1P_1)$ plus CH_4 reaction favors a Mg-insertion mechanism, irrespective of the geometry of the entrance approach.

In contrast to the understanding of reaction dynamics, information on the kinetic data of the $Mg(3\ ^1P_1)$ with CH_4 collision appears to be insufficient. Thus far, Breckenridge

a)Author to whom correspondence should be addressed; electronic mail: kclin@hp9k720.iams.sinica.edu.tw

 © 1998 American Institute of Physics

and co-workers have made the major contribution.[15] Early in the 1980s the authors studied the total deactivation cross sections of $Mg(3\,^1P_1)$ by various small molecules and demonstrated that their quenching behaviors were controlled by entrance channel, in accord with the prediction of long-range attractive interaction. Methane was the only exception in their studies of hydrocarbons, showing a quenching cross section lower than expected from the C_6 correlation. Since the C–H bond strength is greater than 100 kcal/mol of the $Mg(3\,^1P_1)$ electronic energy, they have suggested that the insertion of $Mg(3\,^1P_1)$ into the C–H bond with a slight chemical barrier may account for the discrepancy from the behavior expected by long-range interaction. The *ab initio* potential barrier for the insertion approach was evaluated by Chaqrin *et al.* to be less than 6.9 kcal/mol.[16] The insertion mechanism was energetically favored. The MgH was considered as the major exit channel product in quenching collision, while the energy transfer for $Mg(^1P$–$^3P)$ spin change was not detectable.[15] However, fundamental data such as the reaction barrier, the branching ratio for the chemical and physical quenching, and the temperature effect on the quenching efficiency are still greatly lacking. This work is aimed to conduct these measurements.

In this work, a pump–probe method is employed to determine the thermal rate coefficients of $Mg(3\,^1P_1)$ by collisions with CH_4. The current method is better than the direct measurement of fluorescence decay as a function of quencher pressure. The latter measurement might be bothered by the radiation trapping effect. As reported, the radiation trapping could prolong the measured natural lifetime of $Mg(3\,^1P_1)$ from 1.9 ns to 100–120 ns.[15] The temperature dependence of total quenching rate coefficients is measured over the range from 660 to 850 K. According to the Arrhenius theory, the data obtained are substantially attributed to the chemical reaction with a potential barrier of $-(5.75$–$6.54)$ kcal mol^{-1}. Coupled with the *ab initio* results which find a large barrier to end-on attack, the negative energy dependence indicates that the reaction pathway is along the insertion coordinate, but without the slight potential barrier as reported in the aforementioned studies. Since the effective collision depends on the approach orientation, a simple angle-dependent collision model has been employed to account for the obtained kinetic data.

II. EXPERIMENT

An apparatus similar to the one employed in this work has been described elsewhere,[11–13] so only modification for the present experiment will be described here.

The pump–probe technique is composed of two tunable dye lasers, which were pumped, respectively, by a frequency-doubled and frequency-tripled Nd:YAG laser operating at 10 Hz with pulse duration of 5–8 ns. One dye laser was operated with mixed dyes of rhodamine 590 and rhodamine 610 in a 4:1 volume ratio. The output wavelength of this laser was then frequency doubled through a KDP crystal emitting at 285.2 nm, which was used to excite the Mg vapor in the $3s3p\ ^1P_1$ state. The other dye laser, operated with coumarine 440 emitting at 435 nm, was used to probe the $Mg(3\,^1P_1)$ population in the $3s3p\ ^1P_1$–$3s5d\ ^1D_2$ transition. The nonresonant atomic fluorescence in the $3s5d\ ^1D_2$–$3s3p\ ^1P_1$ transition at 470 nm was detected in order to avoid spectral interference with the incident laser wavelength. The energy of the unfocused pump beam was maintained about 100 μJ for the $Mg(3s3p\ ^1P_1)$ excitation, while the unfocused probe beam was about 50–80 μJ. Each beam was propagated in the opposite direction through an individual pinhole of 10 mm^2 cross section.

Although the energy of the pump laser was kept as low as possible, a weak atomic emission in the $3s4s\ ^3S$–$3s3p\ ^3P$ transition at 517 nm was still detectable. A similar problem was found in our previous work and elsewhere.[10,13] The emission interference might be attributed to resonant two-photon ionization of Mg by the pump laser, followed by recombination and relaxation or electron impact excitation. As it opens the channels for the additional higher lying atomic states populated by the pump laser alone, these collision-induced processes might contribute to the observed fluorescence on the $5d$–$3p$ transition and make the kinetic rate equations, describing the $3p$ population, more complicated. However, these processes were slow, especially for a low pressure condition, and their influence might become significant in a large delay time. For the experimental conditions applied, the fluorescence decay could be characterized exponentially, and therefore interference caused by the processes seems to be negligible in our case.

The reaction chamber was a stainless steel six-armed heat-pipe oven, in which the Mg metal was deposited in the reservoir and heated to a temperature of about 650 K. The Mg vapor pressure in equilibrium corresponded to 1.5 mTorr or 2×10^{13} atoms/cm^3. Mg metal chips were refluxed in the oven at 750 K for about 2–3 h before kinetic measurement. The temperatures of the reactor and the Mg reservoir were measured and regulated by two thermocouples and temperature controllers, respectively. Because parts of the reservoir and reactor were in good thermal contact, the reservoir temperature might rise with the increase of the reactor temperature. In our case, even though the reactor temperature was increased to 850 K, the reservoir temperature might be controlled as low as about 700 K. The generated Mg vapor pressure was still low enough to keep the pseudo-first-order approximation valid.

Methane was the only quencher in the study, but Ar was introduced as a bath gas to keep the methane thermally homogeneous. Methane, 99.999% purity (Matheson), and argon, 99.999% purity (Matheson), were used without further purification. The two gases were regulated by an individual mass flow controller (Sierra Instruments, model 820), well mixed, and then entered the chamber through five side arms. This process ensured that the CH_4 and Ar gases would be mixed well in the oven chamber and that particle deposition on the optical windows would be safely avoided.

Following the $Mg(3\,^1P_1)$ excitation in the presence of excess CH_4 and Ar bath gas, the atomic laser-induced fluorescence (LIF) of $Mg(3\,^1P_1)$ was probed as a function of the time delay between pump and probe beams. The delay time is defined as zero when the falling edge of the pump–laser pulse comes into contact with the rising edge of the probe–

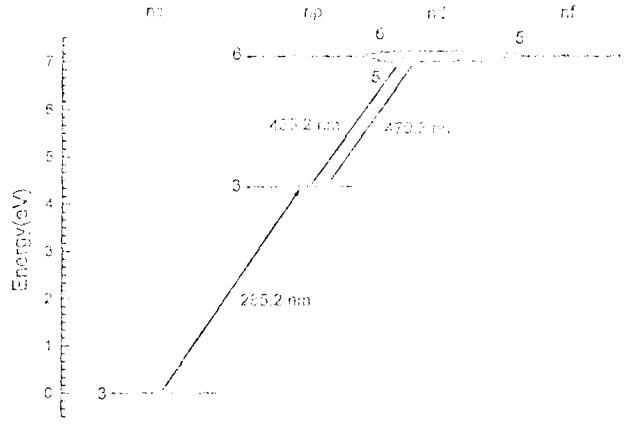

FIG. 1. Atomic energy diagram of Mg. The pump–probe scheme is also displayed with fluorescence detection in the $3s5d\ ^1D_2$–$3s3p\ ^1P_1$ transition.

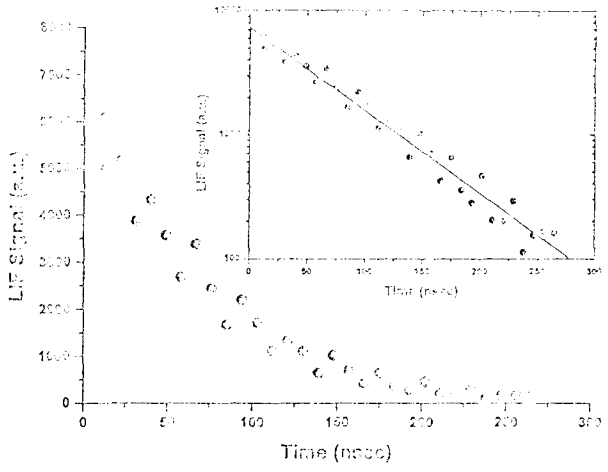

FIG. 2. The Mg atomic LIF decay with the time delay between pump and probe laser pulses. The conditions for the measurement are at temperature 660 K, total pressure 2.5 Torr, and CH_4 concentration 1.29×10^{15} molecule cm^{-3}. Inner panel: Semilogarithmic plot of LIF signal vs delay time. The slope by least-squares fit gives the pseudo-first-order rate coefficient of 2.92×10^6 s^{-1}.

laser pulse. The resulting Mg atomic LIF signal was focused onto a monochromator with a single lens and detected by an attached photomultiplier tube. The grating of the monochromator was set at 470 nm to allow for transmission of a 2 nm spectral bandwidth, when the slits were open to 1000 μm. The LIF signal as a function of time delay was then processed by a transient digitizer (Tektronix, 2432A). To improve the signal-to-noise ratio, each time-resolved spectrum was averaged over 30 traces, and the whole profile was then integrated within a gated width of 400 ns. The data were stored in a personal computer for further treatment.

Figure 1 shows a partial energy-level diagram for Mg[17] and the related transitions for excitation and emission processes. The $3s5d$ state may be populated through radiative or collisional relaxation from $3s6d$ or the intermediate states $3s6p$ and $3s5f$. Thanks to the short lifetimes of these upper states, the involved processes relaxing to the $3s5d$ state have been completed within the 400 ns gated time and the temporal evolution of the $3s5d$ population may decay exponentially with the time delay. The CH_4 pressures were regulated in the range from 20 to 500 mTorr, corresponding to 3×10^{14}–6×10^{15} molecule cm^{-3} in the study. Figure 2 shows an example of time-resolved LIF decay of Mg($3\ ^1P_1$) in the presence of a total pressure of 1.3 Torr which contains 4.74×10^{15} molecule cm^{-3} CH_4 at 660 K. The corresponding effective lifetime may be derived from the slope of the semilogarithmic plot.

III. RESULTS AND DISCUSSION

A. Temperature dependence of the rate coefficients

The depletion of the Mg($3s3p\ ^1P_1$) population by CH_4 collision in the Ar bath gas may be described in the following schemes:

$$\mathrm{Mg}(3s3p\ ^1P_1)+\mathrm{Ar}\rightarrow\mathrm{Mg}(3s^2\ ^1S_0)+\mathrm{Ar}, \quad (1a)$$

$$\mathrm{Mg}(3s3p\ ^1P_1)+\mathrm{CH_4}\rightarrow\mathrm{Mg}(3s^2\ ^1S_0)+\mathrm{CH_4}, \quad (1b)$$

$$\mathrm{Mg}(3s3p\ ^1P_1)+\mathrm{CH_4}\rightarrow\mathrm{MgH}(X\ ^2\Sigma^+)+\mathrm{CH_3}, \quad (1c)$$

$$\mathrm{Mg}(3s3p\ ^1P_1)\rightarrow\mathrm{Mg}(3s^2\ ^1S_0)+h\nu. \quad (1d)$$

The related differential rate equation is expressed as

$$-\frac{d[\mathrm{Mg}]}{dt}=-\{k_{1a}[\mathrm{Ar}]+(k_{1b}+k_{1c})[CH_4]+k_{1d}\}[\mathrm{Mg}]. \quad (2)$$

In our study, we had kept the Mg($3\ ^1P_1$) population density low enough to avoid the self-quenching phenomenon. To apply a pseudo-first-order approximation, we control the partial pressure of CH_4 to be much larger than that of Mg($3\ ^1P_1$) and the total pressure of the system, containing excess Ar bath gas, was maintained constant. The pseudo-first-order decay coefficient, k', is defined as

$$k'=(k_{1a}[\mathrm{Ar}]+k_{1d})+(k_{1b}+k_{1c})[\mathrm{CH_4}] \quad (3)$$

and its value may be determined from the effective lifetime of the atomic LIF decay of the Mg$3\ ^1P_1$ state. Like the example given in Fig. 2, the LIF decays at fixed pressures of CH_4 are exponential with the delay time between pump and probe laser pulses, and their shapes may be fitted to the form of $A\exp(-k't)$. The corresponding effective lifetime may thus be evaluated from the semilogarithmic plot of the decay. The plot of the reciprocal of the effective lifetime, equivalent to k', against $[CH_4]$ yields the intercept, $(k_{1a}[\mathrm{Ar}]+k_{1d})$, and the slope, $k_{1b}+k_{1c}$. Within the temperature range given, the resulting Mg density may lead to radiation trapping, such that the effective lifetime of Mg($3\ ^1P_1$) is prolonged.[15] Since the Ar quenching rate coefficient is negligible as compared to CH_4,[15] and the obtained intercept is small, in Fig. 3, $k'-(k_{1a}[\mathrm{Ar}]+k_{1d})$ vs $[CH_4]$ is plotted over the temperature range of 660–850 K to measure temperature dependence. The slopes of these plots under different temperatures yield the total deactivation rate coefficients, $k_{1b}+k_{1c}$. These data, with 2σ statistical errors from a linear regression fit to each plot, are listed in Table I. In order to examine the reliability of the above method for the effective lifetime detection (Fig. 2), we also monitored the resonance fluorescence from the $3s6d$ to $3s3p$ states at 435 nm at 680 K. The obtained rate

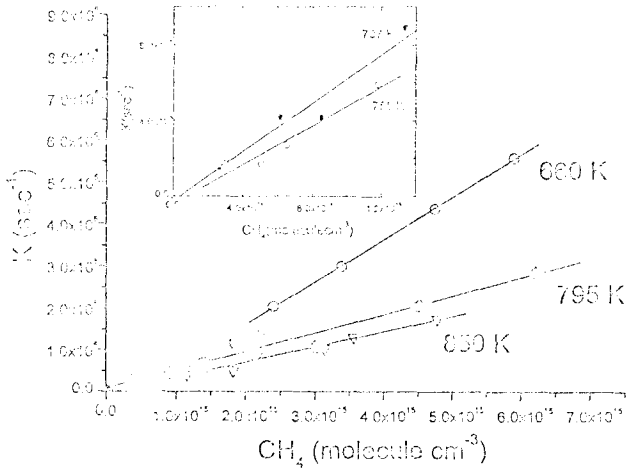

FIG. 3. The plot of K, which is defined as $k'-(k_{1a}[Ar]+k_{1b})$, against $[CH_4]$ at different temperatures. Each slope by least-squares fit gives the second-order rate coefficient.

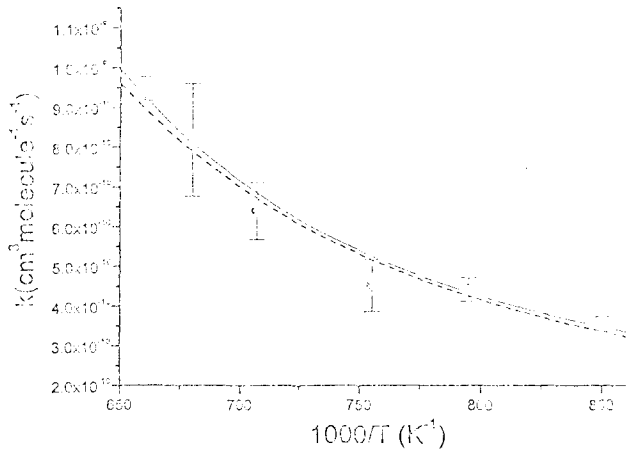

FIG. 4. Temperature dependence of the total quenching rate coefficient, k, for the $Mg(3\,^1P_1)$ atom by CH_4 collision. The solid line indicates the curve fitting to the form of $a+b\exp(-E/RT)$; the dashed line indicates the curve fitting to the form of $b\exp(-E/RT)$ alone.

coefficient was consistent with that evaluated in Table I within 10% deviation. Thus the complication possibly resulting from the reactions initiated by the $3s6d$ state seems negligible in the kinetic rate determination.

The behaviors of physical and chemical quenchings have a different response to temperature variation. The temperature dependence of the physical quenching rate is usually insignificant, especially when the attractive force is dominant. For instance, based on the orbiting model, if the long-range potential is $-C_n/R^n$, the collision cross section for an entrance-channel controlled process can be correlated with the relative collisional energy to a power of $-2/n$.[15,18] The corresponding rate coefficient may be evaluated by integrating the cross section over the full range of collision energies. Two cases are exemplified in the following:[19] (1) For the case of ion-induced dipole interaction, i.e., $n=4$, the resulting rate coefficient becomes temperature independent. The (2) When the interaction of two neutral molecules is dominated by the potential with $n=6$, the rate coefficient is found to depend on the temperature to a power of 1/6. These results reveal that in most cases the temperature factor has little influence on the collision rate coefficients.

In sum, the temperature dependence for the obtained rate coefficients of total deactivation can be characterized by the formula, $k_{1b}+k_{1c}=a+b\exp(-E/RT)$. The first term, related to physical quenching, is assumed to be temperature independent, whereas the second indicates the chemical quenching described by the Arrhenius expression. The values for a fit to the plot of total deactivation rate coefficient versus temperature are: $a=(6.68^{+0.5}_{-1.0})\times10^{-11}$ cm^3 molecule^{-1} s^{-1}, $b=(5.88^{+0.1}_{-0.5})\times10^{-12}$ cm^3 molecule^{-1} s^{-1} and $E=(-6.54^{+0.2}_{-0.2})$ kcal mol^{-1} (Fig. 4, the solid line). The decrease of temperature from 850 to 660 K leads to an increase of the ratio of the chemical to the physical quenching from a factor of 5 to 14. Since the contribution of physical quenching is relatively small, the kinetic data may be fitted alternatively using the Arrhenius expression of $b\exp(-E/RT)$ alone. The plot in Fig. 4 (the dashed line) yields a goodness-of-fit comparable to that in Fig. 4 (the solid line) and the fit gives rise to $k_{1c}=(1.12\pm0.04)\times10^{-11}\exp(5.75\pm1.16\text{ kcal mol}^{-1}/RT)$cm^3 molecule^{-1} s^{-1}. The neglect of k_{1b} apparently has not had much of an affect on the fitted values. This phenomenon reveals the obvious dominance of the chemical reaction over the $Mg(3\,^1P_1)$ depletion channels by the CH_4 collisions. The quenching behavior of $Mg(3\,^1P_1)$ by CH_4 has been considered to be entrance channel controlled.[15] Between the entrance and the exit channel must exist sufficient coupling to let the electronic energy of the excited state be effectively dissipated. Our results indicate that the chemical reaction is the main exit channel. It is worthwhile to note that the thermal rate coefficients are subject to a negative temperature dependence, which indicates that the collision process should be along the attractive surfaces with a depth-well intermediate state.

The chemical interaction of Mg atom insertion into the C–H bond has been demonstrated to be the main pathway leading to the MgH product, of which the rotational distribution is characteristic of a bimodal feature.[7,10,13,14,16] As mentioned earlier, such rotational bimodality originates from the same insertion mechanism, irrespective of the entrance channel geometry. In accordance with Kleiber and co-workers' suggestion,[10] we have recently calculated two-dimensional potential energy surfaces (PESs), when Mg approaches in between two H atoms, and Mg and HCH are coplanar.[13] We found that a nonadiabatic transition had to take part in the reaction to obtain MgH in the $^2\Sigma^+$ state. The low-N and high-N components of the MgH distribution depended on the anisotropic interaction of the final state in the exit channel. The high-N states were anticipated to result from the path-

TABLE I. Experimental determination of thermal rate coefficients k of $Mg(3\,^1P_1)$ by CH_4 collision as a function of temperature.[a]

T(K)	$k(10^{-10}$ cm^3 molecule^{-1} s$^{-1})$	T(K)	$k(10^{-10}$ m^3 molecule^{-1} s$^{-1})$
660	9.48±0.30	755	4.53±0.65
680	8.19±1.42	795	4.43±0.30
707	6.40±0.72	850	3.57±0.18

[a]Quoted uncertainty is 2σ.

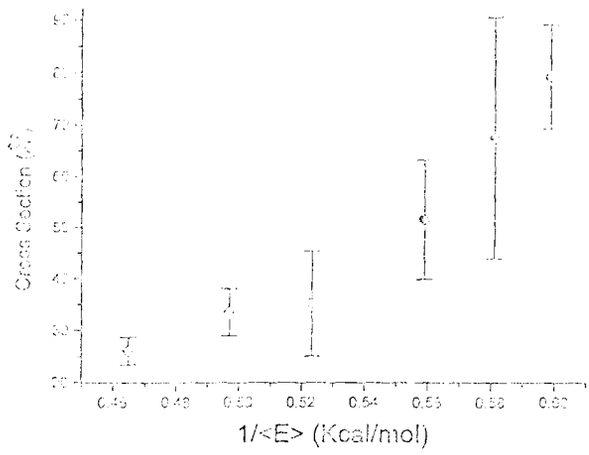

FIG. 5. The plot of total cross section for collisional deactivation against the reciprocal of the relative collisional energy. The cross section is given by the corresponding thermal rate coefficient divided by a mean relative velocity of the colliders, which is $\sqrt{8k_BT/\pi\mu}$.

way that the $HMgCH_3$ collision complex went through—a C_{3v} configuration—before decomposition, whereas the low-N states were formed through the pathway with weaker angular dependence of the potential interaction. By analogy with this case, $Mg(3\,^1P_1)$ with H_2 reaction also leads to a bimodal rotational distribution of MgH.[5,8,9,11,12,20] The subsequent microscopic reaction pathways are similarly dominated by insertion.

Breckenridge and co-workers have investigated the quenching efficiency of the $Mg(3\,^1P_1)$ state by a series of simple gases.[15] They found that except for the inert gases and the perfluoroalkanes, the cross sections were approximately gas kinetic and correlated well with the C_6 long-range force coefficient to a power 0.48 ± 0.05. The obtained value was larger than the prediction of an orbiting model with entirely dispersive long-range force, but could be consistent with an effective potential with a radial dependence between $1/R^6$ and $1/R^4$. Among the saturated and unsaturated hydrocarbons studied, CH_4 was the only quencher with a cross section lower than expected from the C_6 correlation. It was rationalized that a slight chemical barrier might exist for CH_4, but not for the other hydrocarbons.[15]

Since the temperature dependence of the thermal rate coefficients is available, it is worthwhile to examine the applicability of the orbiting model and absorbing-sphere model. Figure 5 shows the plot of the total quenching cross sections against the reciprocal of mean relative collisional energy. The fact that the data cannot be fitted to a straight line implies the invalidity of the absorbing-sphere model in this case. On the other hand, they are not suitable for the orbiting model—which neglects the influence of the reaction orientation. In fact, the chemical reaction in the $Mg(3\,^1P_1)-CH_4$ system will not take place unless the collisions approach the surface crossing region between the excited and the ground state surfaces.

By using a self-consistent field level, Chaquin and coworkers have evaluated the energy barrier along the reaction coordinate to be <6.9 kcal mol^{-1}.[16] The slight barrier, however, has not appeared in our observation of temperature dependence. As pointed out by the authors, the estimated barrier may be lowered considerably provided that a higher calculation level is conducted or the zero-point energy of the departing C–H bond is considered.[16] Their study also shows the existence of a bound state with a productlike structure $MgH\cdot CH_3$ along the reaction coordinate, which lies 12.9 kcal mol^{-1} below the reactants.[16] This singlet bound state, having a small energy gap from the triplet state, enhances the strength of the singlet-to-triplet coupling,[16] thereby accounting for the strong triplet Mg emission observed with the use of Ne-matrix isolation at 12 K.[21] In this work, the resultant negative temperature dependence of the thermal rate coefficients lends support to the prediction of such a bound state, although the observed value is about twice as small as the theoretical energy estimation. In an attempt to find the position of the bound state along the reaction coordinate, it is worthwhile to relate the calculated intermediate structure[16] with two-dimensional PES information.[13] The above bound-state $MgH\cdot CH_3$ is found to be equivalent to the structure of the collision complex in the region of surface crossing. The bond lengths of Mg–H, Mg–C, and C–H in the former structure are 1.75, 2.67, and 2.73 Å, while the corresponding values in the latter one are 1.74, 2.63, and 2.8 Å, respectively. Their geometric structures are in agreement within 5% deviation. It therefore can be affirmed that the bound state is located in the region of surface crossing, since the chemical reaction may not occur unless the nonadiabatic transition is involved.

B. Molecular collision models for the $Mg(3\,^1P_1)+CH_4$ reactions

In this work, we have attempted to fit two simple collision models in the current system. One is a simple collision theory (SCT).[19] Its rate coefficient may be expressed as

$$k_{SCT}(T)=P\pi d^2(8k_BT/\pi\mu)^{1/2}\exp(-E_0/k_BT), \qquad (4)$$

where d is the hard-sphere collision radius; E_0, the energy barrier along the line of centers, which remains constant in the collision irrespective of the orientation; μ is the reduced mass; k_B is the Boltzmann constant, and P is the steric factor. In the equation, the reactants are considered structureless, so that the colliding orientation may not influence the reaction probability. When applying the model, we adopted $E_0=-5.75$ kcal mol^{-1} determined in this work and $d=2.45$ Å for the sum of effective radii of Mg and CH_4. As the steric factor is adjusted to 0.012, a fit is shown in Fig. 6 for the temperature dependence of the rate coefficients. In addition, Eq. (4) is derived by considering the reaction probability as $(1-E_0/E_T)$, where E_T is the relative collisional energy. It becomes questionable to adopt a negative threshold energy in the equation. Although the model fails to apply, the existence of the steric factor might suggest that the anisotropy of the PES should not be ignored.

The other model employed is the angle-dependent line of normals model (ADLN).[19,22] This model attempts to improve the crude isotropic energy barrier of SCT by defining the potential hypersurface to be angle dependent,

$$\epsilon_{th}=\epsilon_{th}^0+2\epsilon'(1-\cos\phi), \qquad (5)$$

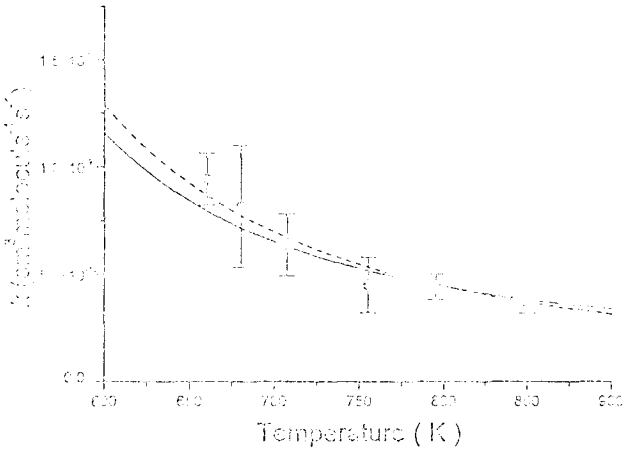

FIG. 6. Curve fit of kinetic data as a function of temperature with the model's SCT (the dashed line) and ADLN (the solid line).

where ϕ is the activated complex bond angle for the colliding system; $\epsilon_{\rm th}^0$ is the threshold energy as $\phi=0$ (i.e., the collision geometry is in the C_{3v} symmetry for the current system); ϵ' is a fitting parameter. The resulting reaction rate coefficient is given as

$$k_{\rm ADLN}(T)=2\pi D^2\left(\frac{8kT}{\pi\mu}\right)^{1/2}\int_0^{\pi/2} e^{-\epsilon_{\rm th}(\phi)/kT}(\sin\phi)\times(\cos\phi)d\phi, \tag{6}$$

where D is the soft-shell reactive radius in the activated complex. In the simulation, we adopted the following values: $D=2.45$ Å, equivalent to the hard-sphere collision radius as described above, and $\epsilon_{\rm th}^0=32.8$ kcal mol^{-1}, evaluated by Chaquin and co-workers[14] in a head-on C_{3v} collision configuration. Under the condition $\epsilon'=-21.6$ kcal mol^{-1}, the rate coefficient measurement may be perfectly fitted (Fig. 6). The predicted threshold energy in Eq. (6) decreases as the angle increases. The tendency is qualitatively consistent with the *ab initio* PES calculation, which reveals that the Mg approach in between two H atoms of CH_4 is energetically favored.[13,16] But it should be noted that the ADLN fit is rough and yields no further information. The model at best reflects a detailed treatment of the steric factor by angular integration over the anisotropic energy barrier.

IV. CONCLUSION

We have obtained the thermal rate coefficients of $Mg(3s3p\ ^1P_1)$ by CH_4 collisions in the presence of Ar bath gas as a function of temperature in the range of 600–850 K. The deactivation processes are attributed to physical and chemical quenching. The former contribution is estimated to be less than 6.7×10^{-11} cm^3 molecule^{-1} s^{-1}, while the latter one is $(0.59-1.12)\times10^{-11}\exp(-5.75-6.54$ kcal mol^{-1}/$RT)$cm^{3}molecule^{-1} s^{-1}. The negative temperature dependence of the measurement indicates the existence of a deep-well intermediate, which is anticipated to locate in the region of surface crossing between the excited and the ground states. Since the reaction is characterized by the anisotropic PES interaction, the orbiting and absorbing-sphere models cannot be validly applied. The ADLN fit to the kinetic data for the temperature dependence is consistent with the insertion mechanism reported, which shows energetic preference to the end-on attack.

ACKNOWLEDGMENTS

The authors wish to thank Dr. D. K. Liu and Y. R. Ou for helpful discussions. This work is financially supported by the National Science council of the Republic of China under Contract No. NSC 87-2113-M-001-021.

[1] B. L. Earl and R. R. Herm, J. Chem. Phys. 60, 4568 (1974).
[2] B. L. Earl, R. R. Herm, S. M. Lin, and C. A. Mims, J. Chem. Phys. 56, 867 (1972).
[3] D. K. Liu and K. C. Lin, J. Chem. Phys. 105, 9121 (1996).
[4] D. K. Liu and K. C. Lin, J. Chem. Phys. 107, 4244 (1997).
[5] W. H. Breckenridge and H. Umemoto, J. Chem. Phys. 80, 4168 (1984).
[6] W. H. Breckenridge and H. Umemoto, J. Chem. Phys. 81, 3852 (1984).
[7] W. H. Breckenridge and H. Umemoto, J. Chem. Phys. 77, 4464 (1982).
[8] P. D. Kleiber, A. M. Lyyra, K. M. Sando, V. Zafiropulos, and W. C. Stwalley, J. Chem. Phys. 85, 5493 (1986).
[9] P. D. Kleiber, A. M. Lyyra, K. M. Sando, S. P. Heneghan, and W. C. Stwalley, Phys. Rev. Lett. 54, 2003 (1985).
[10] T. H. Wong and P. D. Kleiber, J. Chem. Phys. 102, 6476 (1995).
[11] K. C. Lin and C. T. Huang, J. Chem. Phys. 91, 5387 (1989).
[12] D. K. Liu, T. L. Chin, and K. C. Lin, Phys. Rev. A 50, 4891 (1994).
[13] D. K. Liu, Y. R. Ou, and K. C. Lin, J. Chem. Phys. 104, 1370 (1996).
[14] W. H. Breckenridge, J. Phys. Chem. 100, 14840 (1996).
[15] W. H. Breckenridge and H. Umemoto, J. Chem. Phys. 75, 698 (1981).
[16] P. Chaquin, A. Papakondylis, C. Giessner-Prettre, and A. Sevin, J. Phys. Chem. 94, 7352 (1990).
[17] A. A. Radzig and B. M. Smirnov, *Reference Data on Atoms, Molecules, and Ions* (Springer, Berlin, 1985).
[18] J. E. Velazco, J. H. Kolts, and D. W. Setser, J. Chem. Phys. 69, 4357 (1978).
[19] I. W. M. Smith, *Kinetics and Dynamics of Elementary Gas Reaction* (Butterworths, London, 1980), pp. 68–73.
[20] Y. R. Ou, D. K. Liu, and K. C. Lin, J. Chem. Phys. 108, 1475 (1998).
[21] J. G. McCaffrey and G. A. Ozin, J. Chem. Phys. 89, 1844 (1988).
[22] F. L. Wiseman and A. G. Rice, J. Chem. Educ. 70, 914 (1993).

Ab initio calculation for potential energy surfaces relevant to the dynamical formation of MgH($^2\Sigma^+$) in the reaction Mg($3s3p\,^1P_1$)+H_2→MgH($^2\Sigma^+$)+H

Yaw-Pon Ou, Dean-Kuo Liu, and King-Chuen Lin[a)]
Department of Chemistry, National Taiwan University, Taipei, Taiwan 106 and Institute of Atomic and Molecular Sciences, Academia Sinica, P.O. Box 23-166, Taipei, Taiwan 106, Republic of China

(Received 12 August 1997; accepted 13 October 1997)

Two *ab initio* methods have been employed to calculate the dynamical potential energy surfaces (PES's) for the excited ($^1B_2$ or $^1A'$) and the ground ($^1A_1$ or $^1A'$) states in the Mg($3s3p\,^1P_1$)–H_2 reaction. The obtained PES's information reveals that the production of MgH in the $^2\Sigma^+$ state, as Mg($^1P_1$) approaches H_2 in a bent configuration, involves a nonadiabatic transition. The MgH_2 intermediate around the surface crossing then elicits two distinct reaction pathways. In the first one, the bent intermediate, affected by a strong anisotropy of the interaction potential, decomposes via a linear HMgH geometry. The resulting MgH is anticipated to populate in the quantum states of rotational and vibrational excitation. In contrast, the second pathway produces MgH in the low rotational and vibrational states, as a result of the intermediate decomposition along the stretching coordinate of the Mg–H elongation. These two tracks may account for the previous experimental findings for the MgH distribution, which the impulsive model has failed to comprehend. By far, different interpretations have been proposed especially for the low-N MgH product. The supply of a detailed PES's information in this work helps to clarify the ambiguity. It is also conducive to an interpretation of the isotope and temperature effects on the product rotational distribution. © *1998 American Institute of Physics.* [S0021-9606(98)00104-4]

I. INTRODUCTION

The nascent MgH product has been found to yield a bimodal rotational population distribution in the reaction of Mg($3s3p\,^1P_1$) with H_2.[1–6] The reaction pathways to cause such a rotational bimodality has been an issue of concern. As HD was used to replace H_2, the reaction led to an identical MgH rotational distribution. The lack of the isotope effect suggests that the bimodality should originate from a side-on attack of Mg insertion into H_2.[2] In the studies of potential energy surfaces (PES's) calculation, Blickensderfer *et al.* and Chaquin *et al.* have reported that the reaction coordinate for the insertive mechanism trace an attractive $^1B_2$ surface.[7,8] The latter group further demonstrated that the H-abstraction mechanism along a collinear geometry suffered from a substantial energy barrier.[8] The domination of the Mg insertion mechanism was also supported in our experiment of temperature dependence, in that the MgH rotational distribution was little affected with the temperature variation.[3] It is generally anticipated that the Mg($^1P_1$) plus H_2 reaction is exit-channel controlled, causing the MgH rotational bimodality through two distinct microscopic pathways. By analogy with this reaction, Kleiber and co-workers studying the Na($4p^2P$)–H_2 reaction have found a similar rotational bimodality for the NaH product.[9,10] Since there was no kinematic isotope effect on the rotational distribution, the bimodal nature was anticipated to stem primarily from a side-on attack along an attractive surface, which determined the microscopic branching late in the exit channel.

In our recent study of the microscopic branching leading to the MgH product, we have found that two distinct types of reaction dynamics are responsible for the low-N and high-N production.[4] One type produces MgH in lower rotational levels and preferentially $v''=0$, and the other type produces MgH in higher rotational levels with comparable $v''=0$ and $v''=1$ populations.[4] The impulsive model has been adopted for a tentative interpretation on the formation of bimodality. Accordingly, for the major reaction pathway, the H atom is expected to escape from a bent MgH_2 configuration, in which the bending mode initially activated may couple with the asymmetric stretching mode. The energy transfer into the asymmetric stretching mode facilitates the removal of the H atom and causes an effective vibrational motion of the remaining MgH. In addition, a torque is exerted upon MgH to excite the rotational population. As for the minor reaction pathway, the H atom should depart from a linear HMgH intermediate, of which the Mg atom lies in the center. The linear structure in the ground state has been identified to be stable at 12 K.[11] Thus the excess energy carried in the intermediate is presumed to have dissipated before decomposition, and thereby the resulting MgH may stay in the quantum states of low rotation and low vibration.[4]

It should be noted that the impulsive model[12–14] accounts for the breaking apart between the single atom and the remaining diatomic molecule in a three-atom system depending upon the initial bond angle. It ignores the influence of the bond angle variation along the reaction coordinate, and oversimplifies the treatment of potential interaction by using a diatomic potential term instead of a real PES.[15,16] Although the model is easy to follow and sometimes provides satisfactory explanation for the product rotational distribution, its reliability is questionable for the lack of a PES

a)Author to whom correspondence should be addressed. Fax: 886-2-3621483; electronic mail: kclin@hp9k720.iams.sinica.edu.tw

ed.[1] Clearly, for instance, it helps to explain the dramatic difference of the rotational state distributions between OH $^2\Sigma$ and $^2\Pi$ states, which can be derived from the respective $\tilde{B}\,^1A_1$ and $\tilde{A}\,^1B_1$ states of H_2O, in which the initial bond angles are identical for both states.[1,11,12] In the $Mg(3^1P_1)$ plus H_2 reaction, decomposition of a bent MgH_2 structure through a linear geometry may probably lead to rotational and vibrational excitation. However, our previous interpretation, based on the impulsive model neglecting the influence of the angle variation on θ_{cm}, by calculated the formation of low-N components of the MgH distribution to the H-atom release directly from a linear intermediate.[1] In contrast, the high-N component was anticipated to result from the H-atom departing from the bent MgH_2 structure. In the explanation, it is assumed that the restoring force is exerted along the H–H coordinate the Mg atom is treated as a spectator without taking part in the dissociation process. Nevertheless, this assumption turns out to be against the observation of the aforementioned isotope effect.[2] To calculate the related *ab initio* potential energy surfaces is apparently of vital importance to a deep understanding of the reaction mechanisms associated with the rotational bimodality.

Although Breckenridge and co-workers have first suggested that the MgH product rotational distribution should be determined by exit channel dynamics on an anisotropic PES for a decade,[1,2,7] there still lacks a detailed dynamical PES to quantify the related microscopic branching. In this work, we employ two methods of CIS and complete active space self-consistent field (CASSCF) levels to carry out *ab initio* calculation of the dynamical PES's for the excited and the ground states involved in the reaction of $Mg(3^1P_1)$ with H_2. The resulting PES's information supports the mechanism for the MgH production to be through a nonadiabatic transition as proposed previously.[1,4,7,8] However, the prediction of the pathways based on the PES's results is against those on the impulsive model.[1,4] As the $Mg(^1P_1)$ atom approaches H_2 along the $^1B_2$ potential surface, the bent intermediate near the crossing region has been found to decompose following two microscopic reaction processes. As the intermediate decomposition is affected by a strong anisotropy of the interaction potential, the MgH may be produced in the quantum states of rotational and vibrational excitation as observed previously.[1,4] In contrast, as the bent intermediate decomposes along the stretching coordinate of the Mg–H elongation, the pathway produces MgH in the low rotational and vibrational states. Especially for this portion of MgH distribution, different interpretations have been proposed but without the assist of a detailed PES's information. Among these suggestions are the mechanisms via end-on attack of H-abstraction,[1] singlet-to-triplet curve crossing,[8] decomposition of a linear H–Mg–H complex,[1,4] and secondary collision between the rapidly rotating MgH and the product H atom.[1] This work is aimed to clarify the ambiguity from the theoretical point of view and to provide a reasonable interpretation of the isotope and temperature effects on the product rotational distribution.

TABLE I. Comparison of bond lengths and total energies of MgH ($^2\Sigma^+$) and linear HMgH intermediate ($^1\Sigma_g^+$).

Method	Bond length (Å)	Energy	Ref. source
MgH	1.755	[illegible]	[illegible]
	1.726	[illegible]	[illegible]
	1.726	[illegible]	[illegible]
	1.735	[illegible]	[illegible]
	1.741	[illegible]	[illegible]
	1.741		[illegible]
HMgH	1.710	[illegible]	[illegible]
	1.741	[illegible]	[illegible]
	1.701	[illegible]	[illegible]
	1.710	[illegible]	[illegible]
	1.714	[illegible]	[illegible]
	1.713	[illegible]	[illegible]
		[illegible]	[illegible]
		[illegible]	[illegible]

[a]Calculated in the HF/6-31G** level.
[b]Calculated in the CISD/6-31G** level.
[c]Calculated in the MP2/6-31G** level.
[d]Calculated in the MP4/6-31G** level, the method adopted for single point computation of the ground PES in the text.

II. COMPUTATION PROCESSES

A. Method I: CIS

Two methods were employed to compute the potential energy surfaces for the $Mg(3^1P_1)+H_2$ and the $Mg(3^1S_0)+H_2$ systems. In the method I, we used basis sets of 6-31G** level for the Mg and H atoms. The configuration interaction (CI) calculation with single excitation (CIS) contained in the GAUSSIAN 92 program[19] was adopted to compute the $^1B_2$ excited state in C_{2v} symmetry, or $^1A'$ in C_s symmetry for the $Mg(^1P_1)+H_2$ reaction. On the other hand, a fourth-order Møller–Plesset (MP4) method was used to calculate the ground state ($^1A_1$ or $^1A'$) PES for the $Mg(^1S_0)+H_2$ system; the perturbative technique adopted the HF/6-31G** structure as the previous run. A point-by-point calculation was conducted over at least 625 grid points to form a two-dimensional PES each for the excited and ground states.

To test the reliability of the methods used, we computed the structure optimization for MgH ($^2\Pi$ and $^2\Sigma^-$) and HMgH ($^1\Sigma_g^+$ and $^1\Pi_g$). Some calculated bond lengths and total absolute energies are presented in Table I, of which the results are in agreement with those reported previously.[8,20–23] The dynamical PES's for the reactions of Mg ($^1S_0$, ^3P, and $^1P_1$) with H_2 were evaluated in either C_{2v} or $C_{\infty v}$ approach geometry, and the results agree satisfactorily with those from Chaquin *et al.*[8] We also computed the $^1B_2$ and $^3A_1$ surfaces in the Mg–H_2 collisions as a function of bond angle and distance from Mg to the center of H_2. As these two parameters were varied in a linear proportion from the initial C_{2v} to the final $C_{\infty v}$ structure of MgHH, the singlet-to-triplet curve crossing occurred at 30°, a rotation angle of the H_2 molecule around its center. This is also consistent with the result reported by Chaquin *et al.*[8]

TABLE II. Comparison of the calculated energies for the $Mg+H_2$, MgH_2, MgH, and MgH+H species in the ground and excited states.

	CIPSI	CASSCF	HCT	CASSCF
$^1A_1$	[illegible]	[illegible]	[illegible]	[illegible]
$^3B_2$	[illegible]	[illegible]	[illegible]	[illegible]
$^1A_1$	[illegible]	[illegible]	[illegible]	[illegible]

MgH_2	CIPSI	HCT	CASSCF
$^1\Sigma_g^+$	[illegible]	[illegible]	[illegible]
$^1\Pi_g$	[illegible]	[illegible]	[illegible]
$^3\Pi_g$	[illegible]	[illegible]	[illegible]

MgH	CIPSI	CASSCF
$^2\Sigma^+$	[illegible]	[illegible]
$^2\Pi$	[illegible]	[illegible]

MgH+H	CIPSI	CASSCF
$^2\Sigma^+$	[illegible]	[illegible]
$^2\Pi$	[illegible]	[illegible]

[illegible] CASSCF calculation level adopted in this work, CIPSI and HCT adopted by Chaquin *et al.* (Ref. 8).
[illegible] H–H = 0.74 Å; distance from Mg to the center of H_2 = 7.0 Å.
[illegible] H–H = 0.74 Å; distance from Mg to the center of H_2 = 5.0 Å.
MgH = 1.714 Å (CIPSI and HCT) optimized MgH = 1.749 Å (CASSCF).
[illegible] MgH = 1.681 Å (CIPSI) optimized MgH = 1.782 Å (CASSCF).
[illegible] MgH(1) = 1.681 Å, Mg–H(2) = 3.5 Å (CIPSI); MgH(1) = 1.782 Å, Mg–H(2) = 3.5 Å (CASSCF).

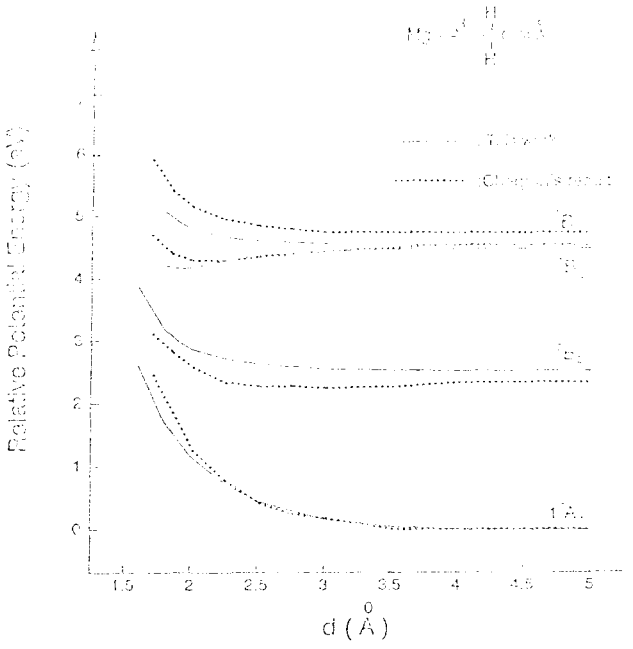

FIG. 1. The potential surfaces for the $1\,^1A_1$, $^3B_2$, $^1B_2$, and $^1B_1$ states, in comparison with those calculated by Chaquin *et al.*

B. Method II: CASSCF

In method II, we employed the CASSCF calculation level with a basis set of 6-31+G* to compute both the ground and the excited PES's for the $Mg+H_2$ reaction.[19,24] Four active electrons and six active orbitals were taken, and the total configurations amounted to 105, which contained not only single excitation but also double, triple, and quadruple excitations. A large increase in the configurations renders method II to be more reliable than method I.[24]

According to this method, the total absolute energies of $Mg+H_2$, MgH_2, MgH, and MgH+H in the varied states were calculated and compared to those reported,[8] as presented in Table II. The CASSCF calculation for the MgH ground state involved three active electrons, five active orbitals, and 40 configurations. The energy optimization for the MgH structure led to a value of 1.782 Å for the bond length and the energy difference of 2.33 eV between $^2\Pi$ and $^2\Sigma^+$ states. The results are consistent with the corresponding findings of 1.731 Å and 2.39 eV, determined from a pertinent emission spectrum.[25,26] For the MgH_2 ground state ($^1\Sigma_g^+$), we adopted four active electrons and six active orbitals in the CASSCF calculation. The optimized bond length of MgH and the total energy yielded a value of 1.7407 Å, and −200.750 48 a.u., respectively. A comparison was made with other results such as bond length of 1.714 Å and total energy of −200.776 66 a.u. from Chaquin *et al.*,[8] bond length of 1.713 Å from Ahlrichs *et al.*,[21] total energy of −200.715 57 a.u. from Pople and co-workers,[22] −200.786 and −200.788 67 a.u. from Ahlrichs *et al.*[21] using PNO-CI and CEPA methods, respectively, and −200.783 86 a.u. from Guest and Wilson.[23] The energies for the MgH_2 excited states ($^3\Pi_g$ and $^1\Pi_g$) were also computed, involving four active electrons, seven active orbitals, and 210 configurations. The obtained energies of the triplet and singlet state relative to the $^1\Sigma_g^+$ ground state were 4.88 and 4.99 eV, close to the values of 5.16 and 5.27 eV reported.[8]

As the $Mg(^1P_1)$ atom approaches H_2 in C_{2v} geometry, the energy level is split into $^1B_2$, $^1B_1$, and $^1A_1$ states. Among them, $^1B_2$ is the only state with an attractive potential, which is stabilized to some extent due to the electronic transfer from $3p_y$ to $\sigma^*_{H_2}$ in the overlap of these two orbitals.[1,8] As compared in Fig. 1, the calculated PES's for $Mg+H_2$ in the C_{2v} approach are consistent with those reported by Chaquin *et al.*[8] While the collision follows $^1\Pi$ or $2\,^1\Sigma^+$ PES's in the $C_{\infty v}$ approach, respectively, Chaquin *et al.* using an extended CI method have calculated the energy barrier to be 1.8 or 1.7 eV.[8] With method II, we obtained a corresponding barrier of 1.67 or 1.36 eV, as shown in Fig. 2. The calculated activation energy is obviously lowered, but there still exists a substantial barrier to prevent from an abstraction reaction along the $C_{\infty v}$ approach.

One should be noted that it becomes difficult to deal with the energy calculation for $Mg+H_2$ (C_s symmetry) near the crossing region, because of the electronic orbital interaction between the ground ($^1A'$) and the excited ($^1A'$) state. In our experience, to choose an appropriate HF wave function seems useful to improve the computation. However, for some grid points in the excited state around the crossing region, where the orbital mixing becomes serious, we have tried to increase the active orbitals up to 7–9, involving three unoccupied $4p$ orbitals of the Mg atom, but still failed to render the corresponding energy converged within 1×10^{-6} a.u.

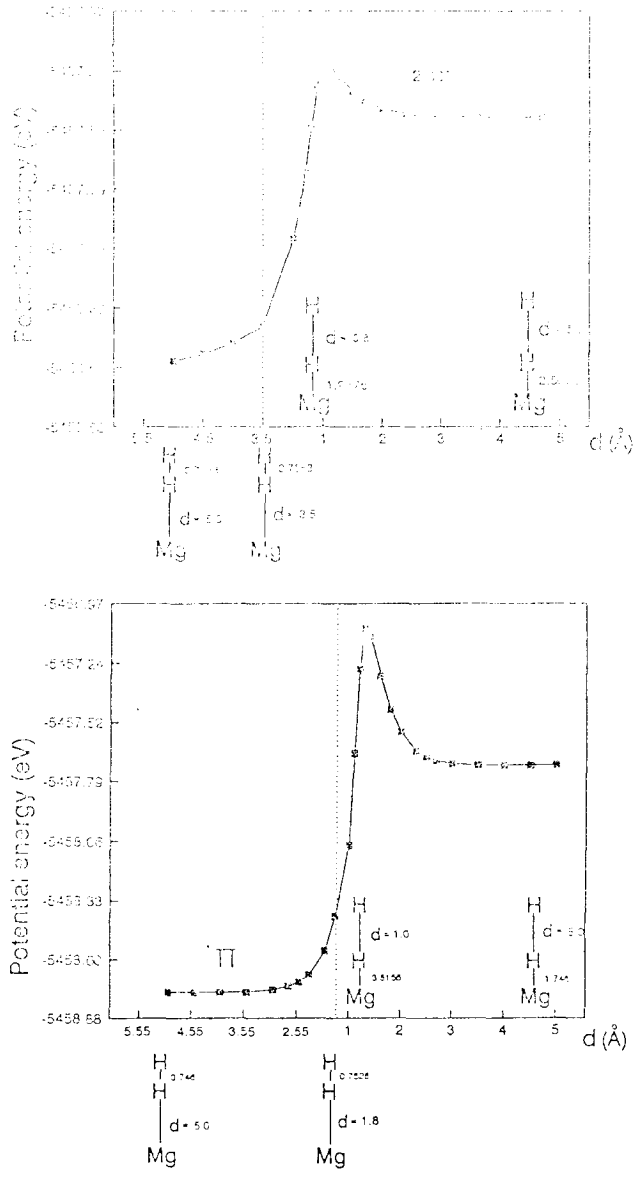

FIG. 2. The behavior of potential energy as $Mg(^1P_1)$ approaches H_2 in a collinear geometry. Note that an energy barrier existing in the $2\,^1\Sigma^+$ and $^1\Pi$ state to be 1.36 and 1.67 eV, respectively.

III. RESULTS AND DISCUSSION

A. Two-dimensional PES's by method I

In Fig. 3, method I was used to compute two-dimensional PES's for the ground ($^1A_1$ or $^1A'$) and excited states ($^1B_2$ or $^1A'$) in the Mg–H_2 reaction as a function of the bending angle α and the MgH distance d, while the other MgH bond was fixed at 1.7345 Å, an equilibrium distance calculated for the ground state. The parameters changed within the range, $35° \leqslant \alpha \leqslant 59°$ and $1.2\ \text{Å} \leqslant d \leqslant 3.96\ \text{Å}$. The upper and lower PES's cross at two regions. Figure 4 shows a detailed description of the equipotential contour of the ground PES, on which the surface crossings are marked. One crossing region (denoted as A) lies within the range of $47° \leqslant \alpha \leqslant 53°$ and $1.6\ \text{Å} \leqslant d \leqslant 2.0\ \text{Å}$, and the other (denoted as B) is within $52° \leqslant \alpha \leqslant 55°$ and $2.2\ \text{Å} \leqslant d \leqslant 2.7\ \text{Å}$. The Mg_2H_2 structure around the larger region A is close to a C_{2v} geometry, having approximately equal bond distances. As the first MgH bond length was theoretically set to 1.5 or 2.1 Å, the corresponding equipotential contour was calculated for the ground state showed the features similar to those in Fig. 4. Although the surface crossings in these cases may have different locations, the intersecting structures around the crossing regions tend to have a near-C_{2v} symmetry.

As mentioned earlier,[1,4,5] the $Mg(^1P_1)$–H_2 collision follows the attractive $^1B_2$ surface and ends up with the production of $MgH(^2\Sigma^+)+H$. The ground ($^1A_1$ or $^1A'$) and excited ($^1B_2$ or $^1A'$) PES's, associated with the $Mg(^1S_0)+H_2$ and $Mg(^1P_1)+H_2$ reactants, correlate symmetrically with the final products of $MgH(^2\Sigma^+)+H$ and $MgH(^2\Pi)+H$, respectively. Therefore, the nonadiabatic transition has to take part in the reaction in order to obtain MgH in the $^2\Sigma^+$ state.[1,4,5] As the $Mg(^1P_1)$ atom approaches H_2 in the C_{2v} geometry, the kinetic energy is initially deposited in the bending mode of $[Mg\text{–}H_2]^*$, which may couple efficiently with the asymmetric stretching mode ($^1b_2$) to induce a vibronic transition;[1,4,5] the $^1B_2$–$^1A_1$ crossing transition is otherwise forbidden.

B. PES information associated with reaction pathways

Schinke *et al.*, without the assistance of a wave packet simulation, have successfully applied the PES calculation as a useful tool to comprehend photodissociation dynamics of polyatomic molecules.[15–17,27] The study reveals that, in the case of so-called "Franck-Condon mapping," in which the final state is weakly affected by the exit channel potential, the resulting product rotational distribution will primarily reflect the initial bending wave function of the parent molecule. But, in the "dynamical mapping," where the final state interaction cannot be ignored, the rotational distribution of the fragment becomes strongly dependent on the anisotropy of the potential energy surface in the exit channel. These concepts, which are known in the field of photodissociation dynamics, are also applicable to a full-collision event.[16] For an exit-channel controlled reaction like the Mg^*+H_2 system, the products are substantially affected by the final state interaction. The supply of a relevant PES information is therefore necessary for understanding the microscopic branching for the MgH population distribution.

To show an explicit relationship between the rotational angular momentum and a torque, we employed a Jacobi coordinate to define the intermediate structure in the Mg–H_2 collision. Under this frame, the variation of the rotational angular momentum in time is related to the torque generated, as expressed by[16,27]

$$\frac{dj}{dt} = -\frac{\partial V(\theta,R)}{\partial \theta}. \tag{1}$$

The equation describes how the rotational excitation depends upon the anisotropy of the relevant PES. Here R denotes the distance between the departing H atom and the center of mass for the MgH product, r is the bond length of MgH, and θ is the Jacobi angle between R and r axes.[16] Since the

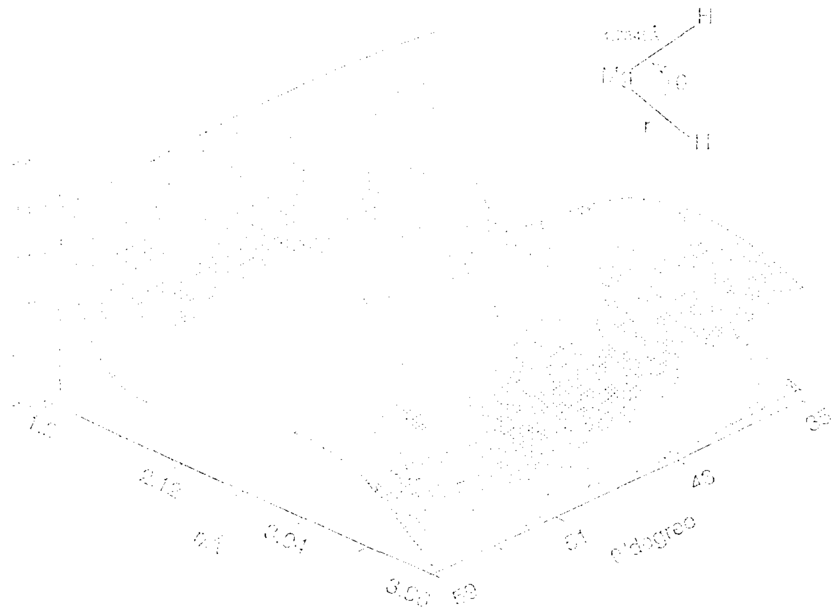

FIG. 3. Two-dimensional PES's for the ground ($^1A_1$ or $^1A'$) and excited states ($^1B_2$ or $^1A'$) in the Mg–H_2 reaction as a function of bending angle and bond distance between Mg and one H atom, while the other MgH bond was fixed at 1.7345 Å. The calculation was conducted with method I.

center-of-mass for MgH lies almost coincidently in the position of the Mg atom, the Jacobi angle may be represented appropriately by the bend angle.

In Fig. 4, two main features may be found from the equipotential contour of the ground PES. First, the potential energy of the ground state rises up at a shorter Mg–H distance, then decreases gradually along the direction of Mg–H elongation. Such a tendency is irrespective of the bending angle. Second, as the angle exceeds about 50° with Mg–H distance close to 1.7 Å, the PES begins to show a strong angular dependence. Once the bending angle is increased to 180°, the potential surface rapidly falls down to the well, 3.8 eV below the reference energy of the Mg($^1P_1$)+H_2 reactants. Accordingly, the MgH_2 complex is anticipated to follow two microscopic pathways to break apart. One tracks along the stretching direction to dissociate Mg–H, and the

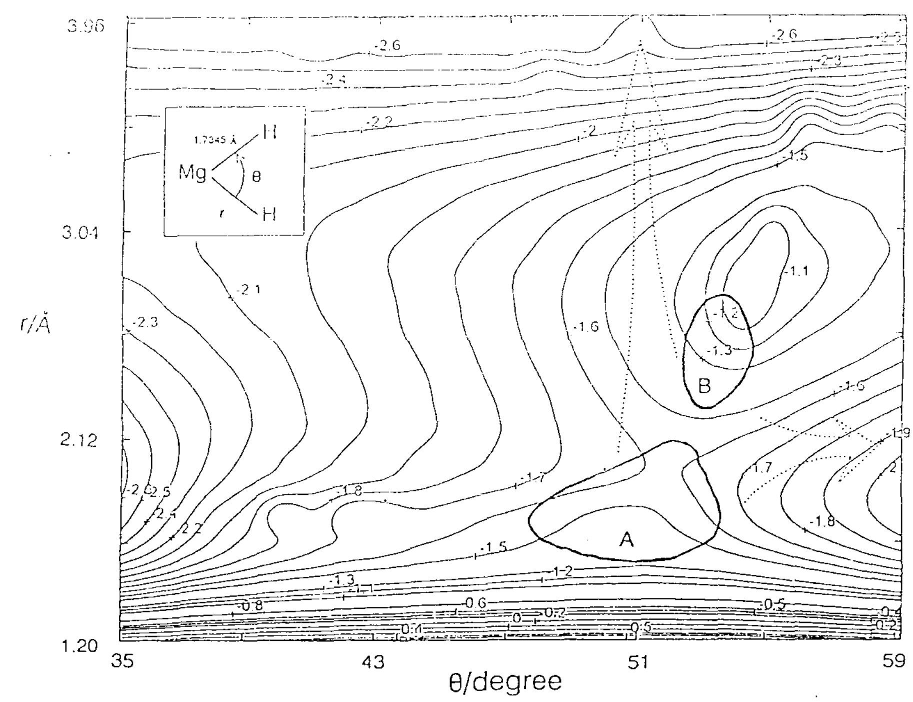

FIG. 4. The equipotential contour (relative energy in eV) of the ground state PES, on which the surface crossing regions with the lowest excited state are marked. The arrows are indicative of the probable exit-channel directions for the H-atom departing from the bent intermediate around the crossing regions.

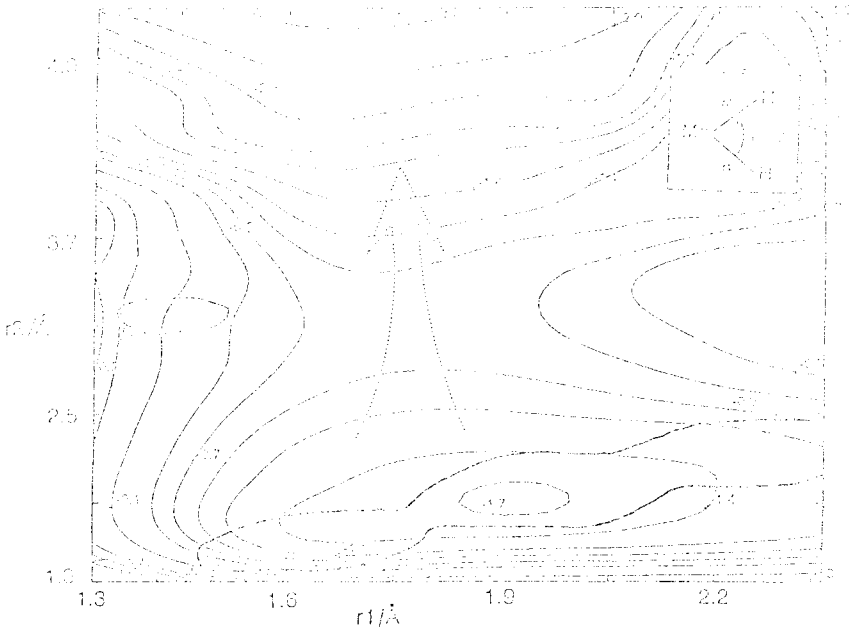

FIG. 5. The equipotential contour (relative energy in eV) of the ground state PES as a function of two Mg–H distances, while the bending angle is fixed at 56°. The heavy circles denote the surface crossing regions, and the arrow is indicative of the probable dissociation direction along the Mg–H coordinate.

other goes through the linear HMgH geometry before breaking apart. If the H atom is removed from the complex along directly the dissociation coordinate of Mg–H, as presented in Fig. 4, the angular dependence of the potential surface will become very weak. Equation (1) shows that the trajectory causes insignificant rotational excitation. Such a dissociation process also results in a weak coupling between the r_1 and r_2 coordinates; that is, when one bond distance r_2 of MgH is prolonged, the other one r_1 maintaining about 1.7–1.9 Å can be little perturbed, as shown in Fig. 5. The final MgH product thus obtained should lie in the low quantum states of rotation and vibration. In contrast, when the dissociation process follows the second trajectory passing through the linear geometry (Fig. 4), a strong angular dependence of the PES results in a large torque, which gives rise to rotational and vibrational excitation for the MgH product. Figure 6 gives a clear depiction of the two reaction pathways. One pathway accounts for the experimental findings for MgH in the lower rotational states and preferentially $v''=0$; the other leads to the higher rotational states with comparable $v''=0$ and $v''=1$ population.[4]

C. PES by method II

As shown in Fig. 7, the potential energies of MgH_2 ($^1B_2$ and $^1A_1$) in C_{2v} symmetry are calculated as a function of the bond length and the bond angle. The nonadiabatic transition may occur within the ranges of bond angle between 40° and 56° and bond distance roughly between 1.7 Å and 2.3 Å. When the angle is fixed at 52°, for instance, the surfaces cross at a Mg–H distance of 2.3 Å. Figure 8 shows the energy of the MgH_2 ground state as a function of bond angle and bond length, when the other bond length is fixed at the optimized distance ~1.7 Å calculated under a C_{2v} geometry. As the $Mg(^1P_1)$ approaches H_2 in a bent configuration, the MgH_2 intermediate is allowed for an effective nonadiabatic transition within a small crossing region as described above. From Fig. 8, the intermediate may be found to dissociate following two pathways. One is to track along the elongation coordinate of Mg–H, which leads to exothermicity at the bond angle <60°. The MgH thus obtained may lie in a low rotational distribution, since the bond angle of MgH_2 is weakly varied as it dissociates. The second pathway is toward the direction of the angle expansion, and thereby the corresponding energy tends to decrease. This channel favors to produce MgH in the higher rotational distribution.

Figure 9 shows the potential energy dependence of the MgH_2 ($^1A'$) ground state on the bond distance, as the bond angle is fixed at 52°. Similarly, the surface crossing is restricted to the range between 1.7 and 2.3 Å. As one bond distance is fixed at 1.775 Å, the MgH_2 becomes ready to dissociate along the MgH stretching coordinate. In this manner, the dissociation process may not disturb the bond angle, thus leading to the low-N MgH product. Furthermore, the bond length at 1.775 Å, close to the equilibrium distance of the product, is little changed during the dissociation. This favors to produce a low vibrational population. The increase of the fixed bond length will hinder the decomposition along the coordinate of MgH elongation. As shown in Fig. 9, when an energy barrier increases with the fixed bond length, the MgH_2 decomposition can follow only the direction via a linear geometry, and the resulting MgH product tends to populate in the higher rotational and vibrational states. Although Figs. 8 and 9 exhibit different aspects from the two-dimensional PES's (Figs. 4 and 5), they provide the same information on the reaction pathways for the MgH distribution.

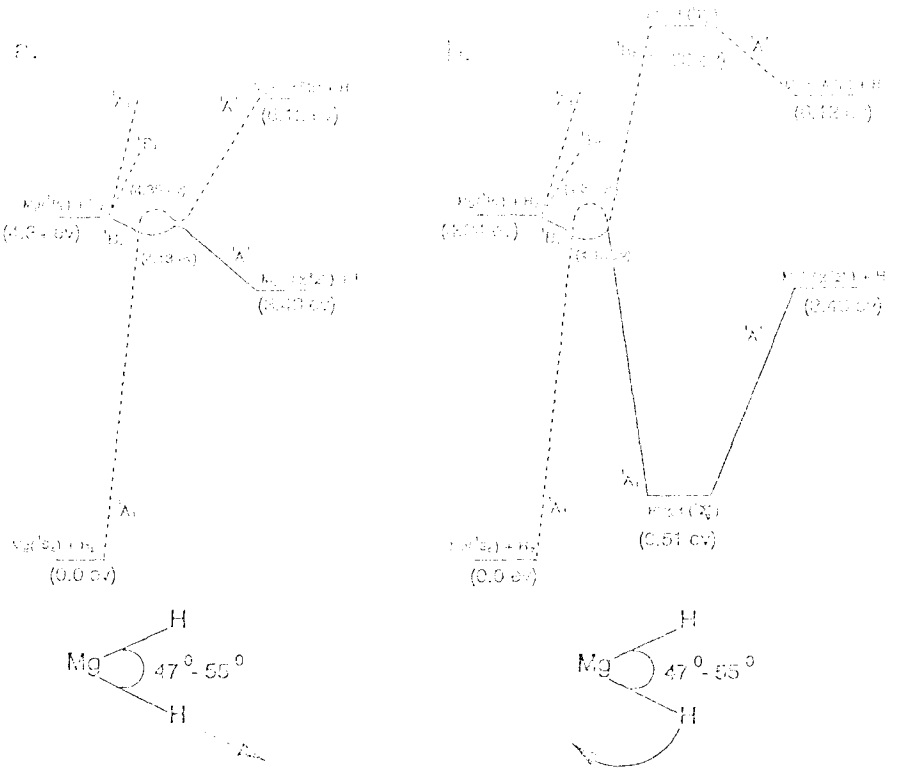

FIG. 6. (a) Reaction pathway that accounts for the previous experimental findings of MgH produced in the lower rotational states and preferentially $v''=0$. The bent intermediate decomposition follows the stretching direction of Mg–H elongation. (b) Reaction pathway that accounts for MgH produced in the high J rotational states with comparable $v''=0$ and $v''=1$ population. The intermediate decomposition passes through a linear geometry. For both pathways, the state energies relative to the $Mg(^1S_0)+H_2$ reactants are calculated with a MP4/6-31G** method. The MgH_2 intermediate near the crossing region is calculated at the bending angle of 50°.

For further conducting quasiclassical trajectory (QCT) calculation, we have applied method II to construct the dynamical PES's for the excited and ground state in the current reaction. The *ab initio* PES's were then converted to an analytic potential energy function, including 34 parameters, using a many-body expansion method.[28] Based on these parameters, a QCT program was performed and led to a bimodal rotational distribution, which is consistent with the aforementioned observation.[1–4] The QCT results confirm the reliability of our PES's computation by method II, and further lend support to the interpretation for the microscopic pathways. We will report the energy function and QCT calculation elsewhere.[29] As shown in Fig. 10, a two-dimensional ground state PES generated from the analytic potential energy function generally agrees with Fig. 4, but presents better quality than that with method I. Again, MgH may be produced via two pathways by means of the equipotential contour of the ground state Mg–H_2. One goes through the linear complex, and the other is along the coordinate of the MgH elongation. The trajectories for the MgH_2 decomposition shown in Fig. 10 are more feasible to recognize than those computed by method I. As mentioned previously, although the PES calculation near the region of the surface crossing is difficult to converge, we have compared the fitting energies with the *ab initio* values computed at the crossing region and the minimum position of the excited state in a C_{2v} geometry. The resulting satisfactory agreement between them assures the reliability of the crossing region shown in Fig. 10. The analytical potential energy function has taken into account ~400 grid points each for the excited and the ground states. The maximum deviation from the *ab initio* energies is 1.5 kcal/mol for the excited state HMgH at a bending angle 12° and 2.0 kcal/mol for the ground state HMgH at 60°. As the worse fitting regions are away from the surface crossing, the quality of QCT performance will not be affected.

D. Isotope and temperature effects

When the excited Mg atom approaches H_2 in a bent configuration, the H–H bond has to elongate to some extent before a nonadiabatic transition takes place. According to the PES calculation, the H–H distance in the MgH_2 intermediate around the crossing region reaches a value between 1.5 and 2.2 Å, much larger than the equilibrium distance 0.74 Å for H_2. When one H atom departs, the restoring force exerted directly on the other H atom may well be negligible. Similarly, in the Mg–HD reaction, HD becomes loosely bonded, when the MgHD intermediate reaches the surface crossing. Thus the D-atom removal may leave insignificant impact on the H atom. This fact accounts for the lack of isotope effect. Of course, we believe that the behavior of isotope effect is more complicated than what we may comprehend. Here we simply provide some insight from the kinematic point of

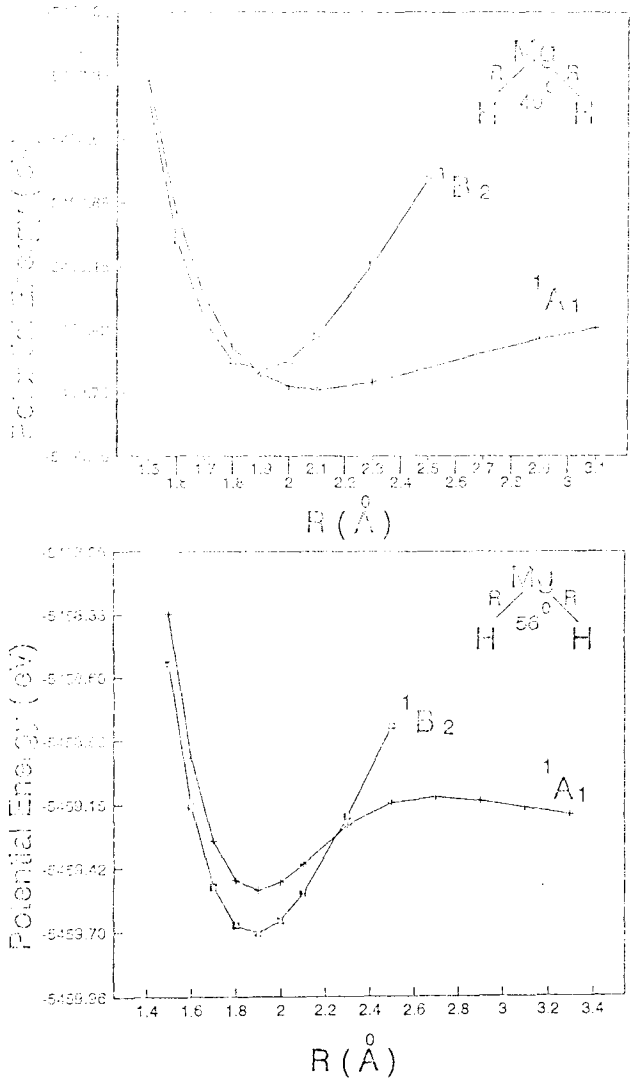

FIG. 7. The potential energies of the MgH_2 complex ($^1B_2$ and $^1A_1$) as a function of bond angle and bond length. Two cases are shown with the bond angle fixed at 40° and 56°.

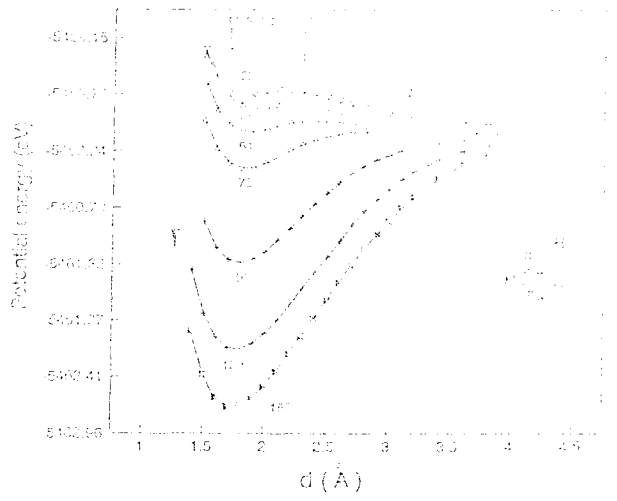

FIG. 8. The potential energies of the MgH_2 ground state as a function of bond angle and bond length, when the other bond length is fixed at the optimized distance = 1.7 Å calculated under a C_{2v} geometry. The surface crossing region is marked. The intermediate decomposition may follow two directions, Mg–H elongation or angle expansion.

view. As to the temperature effect, it may also be rationalized in terms of the PES's information. Since the rotational bimodality originates from the same intermediate in the entrance channel, which in turn proceeds a nonadiabatic transition and then decomposes through two distinct pathways, the low-N and high-N components in the MgH distribution should respond to an identical temperature dependence as observed previously.[3]

E. Impulsive model vs PES

In the light of PES's calculation, validity of the impulsive model may be examined effectively. The pathway leading to the low-N MgH product is taken as an example. In this case, one may find that the H(1)–H(2) bond becomes dissociative when the Mg–H_2 reaches the crossing region, and the bond length of the MgH(1) product is weakly varied throughout the dissociation process. Therefore, the Mg–H_2 interaction potential may well be reduced to only one term of a diatomic potential associated with Mg and the departing H(2) atom, while H(1) is treated as a spectator. Because Mg is much heavier than H, according to the impulsive model, the restoring force along the H(2)–Mg coordinate cannot effectively cause the rotational excitation of MgH(1). Such a prediction is consistent with the interpretation based on the *ab initio* PES for the case of weak anisotropy. The impulsive model becomes reliable in the sense that the PES results meet the required assumption.[12–16]

Nevertheless, the lack of a detailed PES information had misled the mechanism proposed for the low-N MgH distribution to stem from a direct dissociation from a linear HMgH complex.[1,4] Such a consideration is essentially made under the assumption that the linear HMgH is long-lived enough to allow for complete dissipation of the excess en-

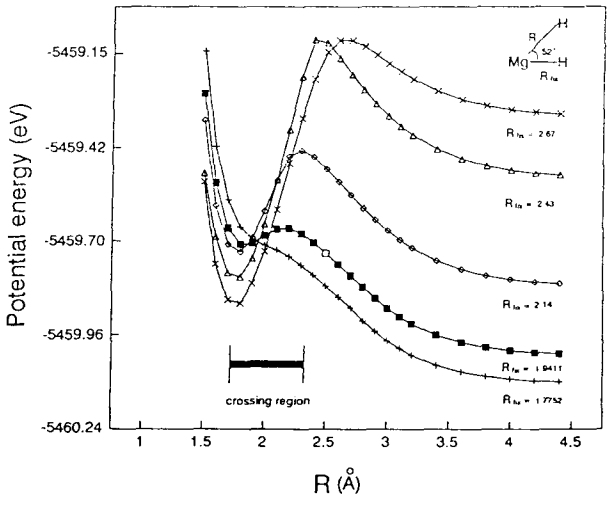

FIG. 9. The energy dependence of the MgH_2 ground state on the bond length, when the other bond length is fixed at various distances, but the bond angle is at 52°. The crossing region with the excited state is marked.

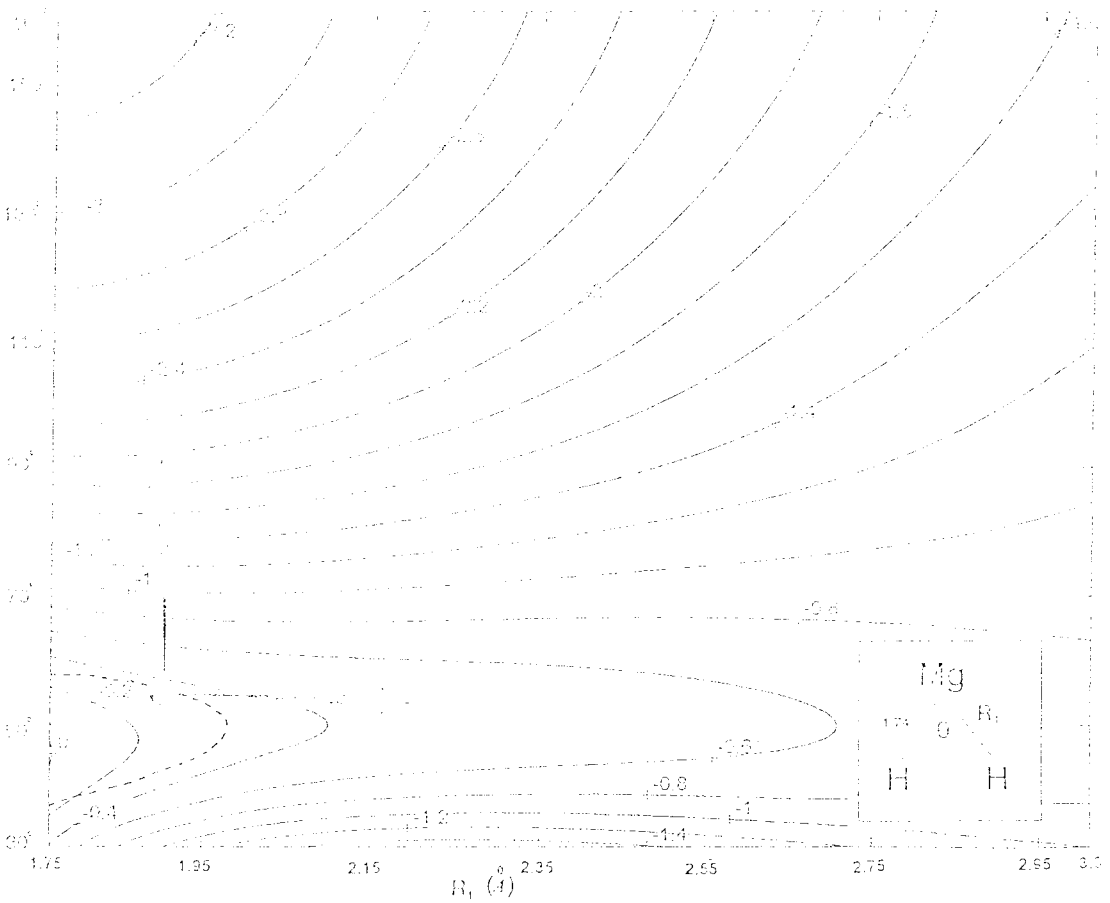

FIG. 10. Two dimensional ground state PES generated from an analytic potential energy function. The dashed circle denotes the surface crossing region and the arrows indicate the probable pathways for the intermediate decomposition.

ergy deposited in the complex before decomposition. But the MgH_2 complex with only three vibrational modes should dissociate rapidly. The prediction by the impulsive model, which ignores the influence of the bond angle dependence, opposes the interpretation based on the PES information.

IV. CONCLUSION

By means of the PES information provided in this work, we may appropriately account for the reaction pathways for MgH produced in the $Mg(^1P_1)-H_2$ collision. As $Mg(^1P_1)$ approaches H_2 in a bent configuration, a nonadiabatic transition has to take part in the reaction to obtain MgH in the $^2\Sigma^+$ state. If the MgH_2 intermediate decomposes along the stretching coordinate of the Mg–H elongation, the resulting MgH may be produced in the low rotational states and preferentially $v''=0$, as observed experimentally. In contrast, if the intermediate decomposition passes through a linear geometry, MgH is anticipated to populate in the quantum states of rotational and vibrational excitation. The isotope and temperature effects on the MgH rotational distribution are also well explained with the calculated PES's. The impulsive model fails to interpret the current reaction, in which the same intermediate is responsible for two distinct rotational and vibrational distributions.

ACKNOWLEDGMENTS

The authors wish to thank Professor C. Witting and Dr. K. Liu for their helpful discussions. This work is supported by the National Science Council of the Republic of China under Contract No. NSC87-2119-M-002-001.

[1] W. H. Breckenridge and H. Umemoto, J. Chem. Phys. **80**, 4168 (1984).
[2] W. H. Breckenridge and J. H. Wang, Chem. Phys. Lett. **137**, 195 (1987).
[3] K. C. Lin and H. C. Chang, J. Chem. Phys. **90**, 6151 (1989).
[4] D. K. Liu, T. L. Chin, and K. C. Lin, Phys. Rev. A **50**, 4891 (1994).
[5] P. D. Kleiber, A. M. Lyyra, K. M. Sando, S. V. Zafiropulos, and W. C. Stwalley, J. Chem. Phys. **85**, 5493 (1986).
[6] P. D. Kleiber, A. M. Lyyra, K. M. Sando, S. P. Heneghan, and W. C. Stwalley, Phys. Rev. Lett. **54**, 2003 (1985).
[7] R. P. Blickensderfer, K. D. Jordan, N. Adams, and W. H. Breckenridge, J. Phys. Chem. **86**, 1930 (1982).
[8] P. Chaquin, A. Sevin, and H. Yu, J. Phys. Chem. **89**, 2813 (1985).
[9] S. Bililign and P. D. Kleiber, J. Chem. Phys. **96**, 213 (1992).
[10] S. Bililign, P. D. Kleiber, W. R. Kearney, and K. M. Sando, J. Chem. Phys. **96**, 218 (1992).
[11] J. G. McCaffery, J. M. Parnis, G. A. Ozin, and W. H. Breckenridge, J. Chem. Phys. **82**, 4945 (1985).
[12] G. E. Busch and K. Wilson, J. Chem. Phys. **56**, 3626 (1972).
[13] D. S. Perry and J. C. Polanyi, Chem. Phys. **12**, 37 (1976).
[14] H. B. Levene and J. J. Valentini, J. Chem. Phys. **87**, 2594 (1987).
[15] R. Schinke, Comments At. Mol. Phys. **23**, 15 (1989).
[16] R. Schinke, *Photodissociation Dynamics* (Cambridge University Press, Cambridge, 1993).
[17] P. Andresen and R. Shinke, in *Molecular Photodissociation Dynamics*,